Pergamon

*Int. J. Heat Mass Transfer.* Vol. 39, No. 10, pp. 2149–2164, 1996

0017-9310/96 $15.00 + 0.00

0017-9310(95)00294-4

# Velocity near-field of variable density turbulent jets

M. AMIELH, T. DJERIDANE, F. ANSELMET and L. FULACHIER

IM2, Université d'Aix-Marseille II, Institut de Mécanique Statistique de la Turbulence, 12 avenue du Général Leclerc, 13003 Marseille, France

(*Received* 13 *December* 1993 *and in final form* 27 *June* 1995)

**Abstract**—An experimental investigation of the near-field region of variable density turbulent jets is presented. The velocity measurements are performed using a two-component laser Doppler anemometer in an axisymmetric jet of helium, air or $CO_2$ exhausting into a low-speed air coflow. Pseudo-similarity considerations, using the initial density ratio, give a good collapse of the mean axial velocity evolutions for gases with very different densities. The comparison of the statistical moments up to the fourth-order confirm that the development of a lower density gas is more rapid than that of a heavier gas with either the same exit momentum flux or at the same Reynolds number. Copyright © 1996 Elsevier Science Ltd.

## INTRODUCTION

One of the main objectives of this paper is to provide reliable velocity experimental data, allowing a better understanding of the influence of density variations on the structure of turbulence in the near-field region of jets. In particular, for such flows, the conservation equations for thermodynamics, mass and momentum are linked together through density variations. This feature significantly enhances the difficulty of refined flow modelling and requires experimental efforts to make available strong guidelines for the development of well suited modelling [1, 2]. In addition to the fundamental problems involved, such as the possibility for such flows to generate self-excited oscillations for sufficiently low Reynolds number [3], studying flows with strong variations of density is important for many practical situations, such as the aerospace industry, pollution and environmental problems, engine combustion chambers... This can also be the key to an improved understanding of turbulent flows with combustion, where the coupling between reactions and aerodynamics occurs through the localized density fluctuations introduced by chemical heat release [4].

If this relatively basic configuration has already received attention for the study of the far-field [2, 5], the near-field was mainly investigated through the scalar mixing [6, 7] and rarely through the velocity field in the same experiment [8]. So, the dynamic behaviour of turbulent jets near the nozzle exit was not clearly described in the presence of strong density variations. The main difficulty encountered in such flow investigations is that simultaneous measurements of the velocity and the density are difficult to perform. In the present paper, only the velocity field is described. A total of 10 sections from the exit up to 30 nozzle diameters are investigated in helium, air and $CO_2$ turbulent jets.

Though it has been shown that an exact similarity cannot be attained in such flows [9], the axial evolution of some of the dynamical characteristics is well predicted by approximated laws, taking into account the initial density ratio $\rho_j/\rho_e$ and the relative importance of the involved three different forces known as the inertial, gravitational and viscous ones. However, in this near-field region where the initial conditions, such as in particular the Reynolds number, still play a role in the jet development, the confinement and the coflow are also other parameters which need to be considered in order to approach the specific effects of strong density variations on the jet development. The influences of all these parameters are actually addressed in the present paper.

## 1. EXPERIMENTAL SET-UP

### 1.1. *Experimental facility*

Experiments described herein are performed in a 12 m high, vertical wind tunnel with ascending blowing. The flow facility consists of an axisymmetric 26 mm diameter pipe jet of helium, air or carbon dioxide which exhausts with fully turbulent developed conditions into a low speed coflowing air stream (Fig. 1, [10]). This allows a large variation of the initial density ratio between the jet fluid and the coflow, namely, from $\rho_j/\rho_e = 0.14$ for the helium jet to 1.40 for the $CO_2$ one. According to experimental requirements for performing two-dimensional laser-Doppler velocimetry, the Plexiglas duct which weakly confines the flow field ($S_e/S_j > 120$) can have either a 285 mm diameter circular section or a 285 mm side squared section. This transparent part is high enough (1.2 m)

## NOMENCLATURE

$D_{ef}$ effective nozzle diameter
$D_j$ internal nozzle diameter
$Ct$ Craya–Curtet number

$$Ct = \frac{U_k}{(U_d^2 - \frac{1}{2}U_k^2)^{1/2}}$$

with

$$U_k = \frac{\rho_j U_j D_j^2 + \rho_e U_e (D_e^2 - D_j^2)}{\rho_0 D_e^2}$$

$$U_d^2 = \frac{\rho_j U_j^2 D_j^2 + \rho_e U_e^2 (D_e^2 - D_j^2)}{\rho_0 D_e^2} - \frac{1}{2}\frac{\rho_e}{\rho_0} U_e^2$$

$$\rho_0 = \frac{\rho_j U_j D_j^2 + \rho_e U_e (D_e^2 - D_j^2)}{U_j D_j^2 + U_e (D_e^2 - D_j^2)}$$

$Fr$ Froude number,

$$Fr = \frac{\rho_j U_j^2}{g D_j |\rho_j - \rho_e|}$$

$k$ turbulent kinetic energy
$L_u$ velocity half-width, radius where $U - U_e = 1/2(U_c - U_e)$
$R$ radial co-ordinate
$S$ area
$U, U, u$ axial velocity, instantaneous, mean and fluctuation
$V, V, v$ radial velocity
$W, W, w$ azimuthal velocity
$U_{ce}$ axial velocity used for the pseudo-similarity evolution that takes into account the coflow influence, $U_{ce} = \sqrt{U_c^2 - U_e^2}$
$X$ axial co-ordinate.

Greek symbols
$\rho$ gas density.

Subscripts
$c$ on the jet axis
e external, refers to the coflow
j on the jet axis, at the nozzle exit
$u$ refers to the $U$-component
1 refers to the inertial zone
2 refers to the intermediate zone
$( )'$ root mean square, $u' = (\overline{u^2})^{1/2}$.

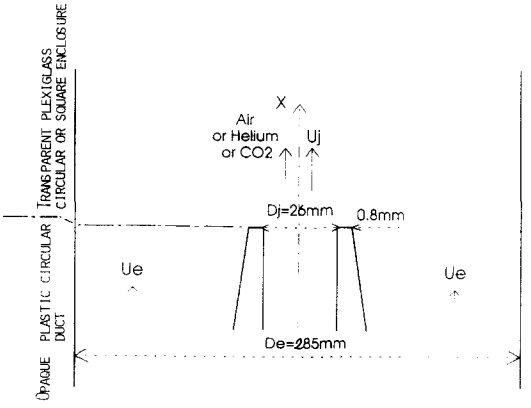


Fig. 1. Details of the exit nozzle.

to allow a study of the turbulent mixing up to 40 diameters $D_j$ from the nozzle exit.

The primary air jet is supplied by an upstream blower with a mass flux deduced from the static pressure difference induced by a Venturi effect. This pressure variation is given by a Furness Control differential micro-manometer in the $\pm 19.99$ mm $H_2O$ range. It is directly linked with the primary velocity in the nozzle exit and consequently with the mass flux using a separately performed calibration.

The blow-off of some 200 bars pressurized helium gas or of some 50 bars pressurized liquid carbon dioxide storage tanks is used to supply the primary jet of helium or $CO_2$. Due to the room being occupied by the tanks and for safety reasons, the storage is located outside of the laboratory. The flow is conditioned at ambient pressure and temperature by traversing several expanders and copper air–gas exchangers. Moreover, a vaporizator is needed for the carbon dioxide to transform this fluid into the gaseous phase. For these two gases, the mass flux rate is fixed by a digital selection on two Shaefer flow controllers, connected in parallel, which regulate with an accuracy better than $\pm 1.5\%$. The primary temperature is controlled by 100 Ohm platinum resistances placed in several sections ahead of the nozzle exit. The primary gas is selected by acting on automatic valves monitored, as most of the electric systems controlling the facility, from the control panel located in the experimental room.

For the three gases, the primary flow develops in a 4 m long pipe with a 38 mm diameter for the first 2 m and a 26 mm diameter for the last 2 m after a contraction section. The primary flow is a fully turbulent pipe jet so that no turbulence transition has to be considered in the studied zone. Moreover, a high enough Reynolds number for the helium jet ($Re_j > 4500$) and the presence of the coflowing stream prevent any self-sustained oscillations developing in the jet, like those described by Huerre and Monkewitz [3] when $\rho_j/\rho_e < 0.72$. Then, the initial chosen con-

Table 1. Nominal experimental conditions

| Gas | $U_j$ (m s$^{-1}$) | $Re_j$ | $\rho_j/\rho_e$ | $Fr_j$ |
|---|---|---|---|---|
| He | 32 | 7000 | 0.14 | 643 |
| Air | 12 | 21 000 | 1 | |
| $CO_2$ | 10 | 32 000 | 1.4 | 1363 |

ditions agree with the most often encountered industrial situation. The thickness of the exit nozzle is 0.8 mm. The superposition of a honeycomb, five grids and a metallic wool tampon inside the primary pipe permits good control of the velocity turbulence level (4%) at the nozzle exit, which compares favourably well with the turbulence level in the usual turbulent pipe flows [11]. Turbulence in the external boundary layer (28 mm thickness in the exit section) of the secondary flow is created by 2 mm high roughness elements located $10D_e$ upstream of the exit section.

The coflowing or secondary stream is entrained by the primary jet and drawn up by a blower located 200 diameters $D_j$ downstream of the jet ejection. For safety reasons, both this sucking blower which ejects the mixed gases outside of the room and a confinement zone on the ground of the wind tunnel are required when using carbon dioxide. The coflowing velocity, about 1 m s$^{-1}$ in the middle of the gap, is directly known by measuring dynamic pressure with a pressure tube and temperature with a 100 Ohm platinum resistance located 1 m upstream of the nozzle exit. Another control of the secondary temperature is systematically made using a similar resistance in the $X/D_j = 0$ section, at the radial location $R = 100$ mm. For the present experiments, the coflow is essential for providing reliable measurements at the jet edge using laser velocimetry, in particular since this allows the simultaneous seeding of both streams. The secondary velocity is chosen low enough to prevent any strong perturbation of the primary jet development, but it must be high enough to avoid the development of any reverse flow in the studied zone. The latter feature is assumed to be ensured when the Craya–Curtet number $Ct$ extended to variable density flows is larger than 0.8 [12], whatever the gas. The nominal experimental conditions correspond to an exit momentum flux of 0.1 N for the three gases (Table 1). This choice is motivated by physical considerations since this ensures identical initial forces for the three involved gases. In addition, visualizations performed by Pitts [6] show that an air jet and a helium jet present a similar global structuration for the same momentum flux, whereas they look totally different for the same Reynolds number. Numerical results recently obtained by Ruffin *et al.* [1] confirm that the main parameter which governs the turbulent mixing through the different turbulent scales is effectively the exit momentum flux. So, the choice of the momentum flux as the control parameter between the considered experiments is well justified. The fact that the secondary mass flux is maintained constant between the round and the squared ducts induces a decrease of the nominal coflowing velocity $U_e$ from 1.2 to 0.9 m s$^{-1}$. With these conditions, the mixing flow is investigated only in the region where gravitational forces are not predominant. The two zones mainly studied are the so-called [9] inertial zone, including the potential core, where momentum forces predominate, and the intermediate zone, where gravitational forces are not negligible anymore and have to be taken into account for the data analysis. This near-field region is still far from the plume conditions which begin far beyond the station where measurements are stopped ($X/D_j = 40$). Indeed, gravitational forces would be theoretically predominant from $X/D_j > 73$ and $X/D_j > 170$ in the helium and $CO_2$ jets, respectively.

### 1.2. *Laser velocimetry*

Velocity measurements are performed with a laser Doppler system using the two colour beams at the 488 and 514.5 nm wavelengths of a Spectra Physics 4 W argon laser source. The light is transmitted from the source to the emission–reception head by 10 m long optical fibers, and back scatter detection is used. This arrangement is necessary to avoid tedious tuning of the optics when the measurement point is moved, and is essential for experiments with helium. Three beams, the blue, the green and the common one (containing both the blue and green colours), are emitted from the head. The distance between any two beams at the head exit is 49.7 mm. The probe measuring volume ($0.12 \times 0.12 \times 1$ mm$^3$) is located at a 310 mm focal distance from the head. An automatic plane traversing mechanism ensures the volume location with more than 1/100 mm accuracy. The two orthogonal fringe planes are inclined with a 45° angle towards the vertical jet axis in order to obtain an equivalent sensitivity on the two velocity components. The flow direction is distinguished by implementation, through a bragg cell, of a 40 MHz frequency shift on both the blue and green beams. Then, the combinations $\mathcal{U} + \mathcal{V}$ (or $\mathcal{W}$) and $\mathcal{U} - \mathcal{V}$ (or $\mathcal{W}$) are simultaneously measured. The various statistical moments of $\mathcal{U}$, $\mathcal{V}$ and $\mathcal{W}$ are calculated up to the fourth-order.

The primary and secondary streams are seeded with a silicone oil aerosol such that the particle diameter is around 1 $\mu$m. Seeding is realized by injecting pressurized air into the silicone oil stored in glass-blown particle diffusers similar to those used in perfume diffusion. The air flux injected in the primary flow is 1.2 l min$^{-1}$ ($2.10^{-5}$ m$^3$ s$^{-1}$), so that the primary gas dilution is negligible, in particular for the helium jet where the volume fraction is still 99.9%. The primary flow is seeded at the wall at $150D_j$ upstream of the nozzle exit. For the secondary stream, the aerosol is injected at the convergent entry. Consequently, a homogeneous seeding is obtained in the secondary flow and especially around the primary jet side, which allows measurements on the edges of the jets to be performed.

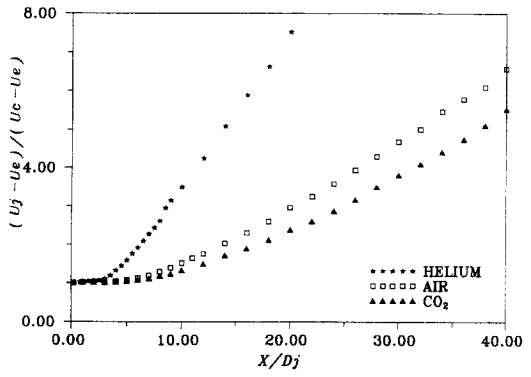


Fig. 2. Decay of the mean streamwise velocity along the jet axis.

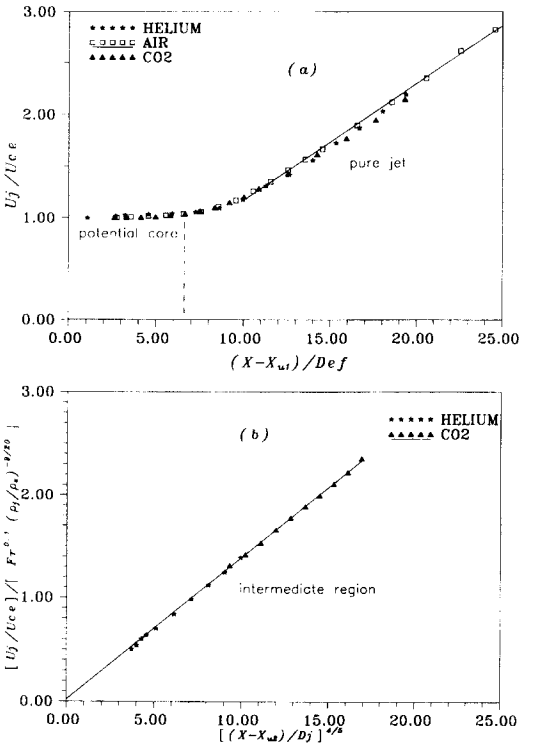


Fig. 3. Evolution of the mean streamwise velocity using the pseudo-similarity laws suggested by Chen and Rodi [9]: (a) pure jet region, $U_j/U_{ce} = 2A[(X-X_{u1})/D_{ef}]$ with $A = 0.055$; (b) intermediate zone, $U_j/U_{ce} = K_u Fr^{1/10}(\rho_j/\rho_e)^{-9/20}[(X-X_{u2})/D_j]^{4/5}$ with $K_u = 0.138$.

Two Burst Spectrum Analysers connected to an Olivetti SX20 computer by an IEEE card process the Doppler signals through the Dantec 'Burstware' software. For each colour, 7000 bursts are recorded. Thus, the various statistical moments are computed with about 5000 points, because only the detections within a coincidence window based on an arrival time difference lower than or equal to 2 $\mu$s are kept for the calculation. In order to check the validity of these measurements, ponderations of moments using characteristical times of the recorded bursts were calculated. No significative discrepancy was observed between the bursts' arrival time weighted mean velocity and raw mean velocity, probably because of the arrival time randomness. On the contrary, weighting with the particle transit time in the probe volume induced great differences on the mean velocity and gave in particular some incoherent results for the mean radial velocity $V$ and, more precisely, for the gradient $\partial V/\partial R$ when compared with results inferred from the continuity equation using the measured $U$ distributions. So, velocity results presented hereafter are raw velocity results.

## 2. RESULTS AND DISCUSSION

### 2.1. *Centreline profiles*

2.1.1. *Mean longitudinal velocity*. Figure 2 presents the axial evolution, as a function of the downstream distance $X/D_j$, of the mean streamwise velocity $U_c$ for the three gases using the usual non-dimensional presentation $(U_j-U_c)/(U_c-U_e)$. The influence of density differences is obvious, showing that the centreline fall-off is much greater for He that for air and $CO_2$: light gases tend to mix more quickly with the ambient one than heavy gases do. However, many parameters other than the density variation may induce such a behaviour. Gladnick *et al.* [13] show that the velocity decay is also linked, in particular, to the initial ratio $U_j/U_e$ and the exit nozzle velocity profile shape. With the presently chosen conditions, $U_j/U_c$ is found to be higher for the helium jet than for the two other gases ($U_j/U_c = 36$, 13, 11 for the helium, air and $CO_2$, respectively, when using the squared enclosure), so that this may affect the axial velocity decay in the same way as low density does.

Nevertheless, if the coflowing velocity is taken into account in the momentum equation, Sautet [14] indicates that the similarity laws proposed by Chen and Rodi [9] give a good collapse of the centreline axial velocity decay laws for gases with very different densities, but using $U_j/U_{ce} = U_j/(U_c^2-U_e^2)^{1/2}$ instead of $U_j/U_c$ as in free jets. In addition, when using the Froude number, the separation between the inertial and intermediate zones is located on the axis at the abscissa given by $X_1/D_j = Fr^{-1/2}(\rho_j/\rho_e)^{1/4}X/D_j = 0.5$, corresponding to $X/D_j = 7.5$ and 20, for the helium and $CO_2$ jets, respectively. Then considering whether the gravitational forces are negligible or not, two different laws describe the centreline axial velocity decay. The good agreement of these laws for the three gases in the two main zones is shown in Fig. 3. The relevance of the effective diameter $D_{ef} = D_j(\rho_j/\rho_e)^{1/2}$, as firstly introduced by Thring and Newby [15] for collapsing the data, is confirmed in the momentum dominated zone ($X < X_1$). Other effective diameters based on global densities defined with the momentum or the concentration profile [4, 14] have been checked not to be so good. The resulting coefficient for the decay of the axial mean velocity using $D_{ef}$ is about 0.055 in the inertial region, in the lower range of

the values usually reported in the literature, which lie between 0.05 and 0.08 and are often relative to free jets (e.g. Ruffin *et al.* [1], Fulachier *et al.* [4]). This is not unexpected since the slope of the axial velocity decrease is generally higher in free jets. Indeed, additional measurements performed in our facility for free jets of air and helium give the slopes of 0.085 and 0.069, respectively. By comparison, Panchapakesan and Lumley [2] found 0.082 in an air free jet and 0.076 in a helium free jet, so, even if the external velocity and the confinement can be considered as weak according to the initial conditions, they slightly hinder the jet development.

The associated virtual origin $X_{ul}$ is negative and directly related to the potential core length which is shorter for the lighter gas ($X_{ul}/D_j = -0.2$, $-2.6$, $-2.9$, respectively for the helium, air and $CO_2$ jets in the momentum dominated region). Due to geometric considerations, the virtual origin is different in the pure jet region and in the intermediate region. In the latter one, buoyancy effects are not negligible anymore ($X > X_1$) and the centreline axial velocity decay then follows a non-linear evolution corresponding to the empirical expression [9] $U_j/U_{ce} = K_u Fr^{1/10}(\rho_j/\rho_e)^{-9/20}[(X-X_{u2})/D_j]^{4/5}$, where $K_u$ is the same for He and $CO_2$. The present value of $K_u = 0.138$ is identical to that given by Chen and Rodi [9] in their study of free jets. Finally, the representations of Fig. 3 show that the previously evoked parameters such as the $U_j/U_e$ ratio, the exit velocity profile shape or even the Reynolds number have a rather small influence on the centreline axial velocity decay, compared to that due to the density variations. It is worth noticing that the collapse of the three velocity evolutions provided by this representation is almost perfect for the very near-field region, where the flows are far from being completely developed and the assumptions usually used for the pseudo-similarity approach are far from being valid.

2.1.2. *Velocity turbulent intensity.* The evolution of the centreline velocity turbulent intensity is presented in Fig. 4a. Here again, in the near-field region, the increase of $u'/(U_c-U_e)$ is much more rapid for the helium jet than for the air jet. In order to distinguish between the Reynolds number and the density variation effects, the centreline velocity turbulent intensity was also measured in an air jet with a 7000 Reynolds number. Even though the increase of $u'/(U_c-U_e)$ is then more rapid than for the air jet with the 21 000 Reynolds number, the maximum level of this turbulent intensity remains lower than that for helium jet in the investigated region. Thus, it appears that a lower Reynolds number and a lower density induce a similar effect on the development of the jet, but the effect of the density variation is significantly stronger than that of the Reynolds number.

In the present measurements, an asymptotic value of 27% for $u'/(U_c-U_e)$ is reached at $X/D_j = 5$ in the helium jet, whereas such a plateau is not yet obtained at $X/D_j = 30$ for the two other gases. However, it seems that this value of 27% would be reached for all

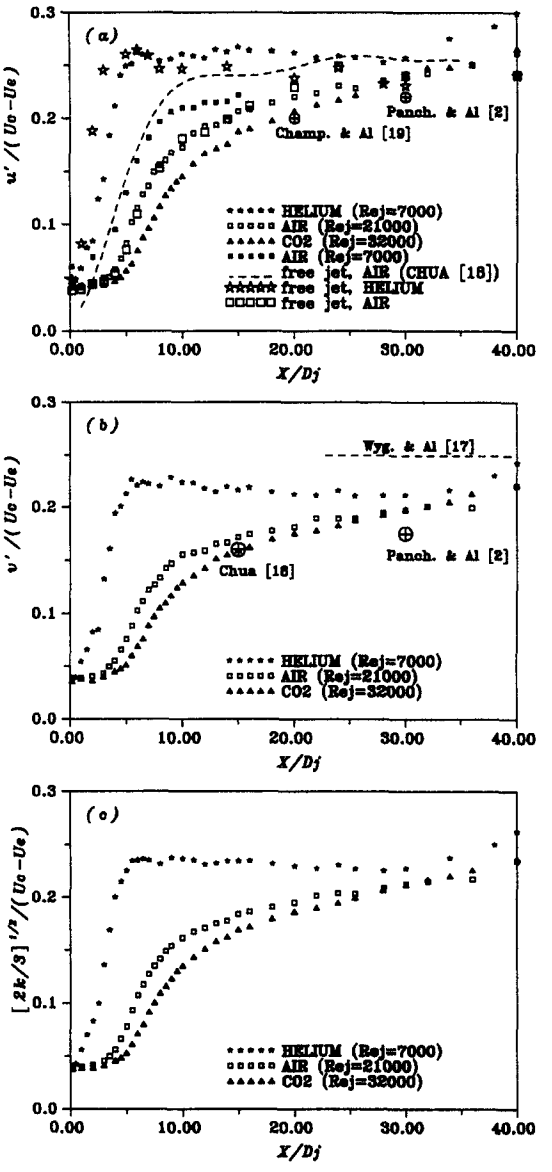


Fig. 4. Turbulence intensities along the jet axis (comparison with data in free air jets of Wygnanski and Fiedler [17], Chua [18], Champagne and Wygnanski [19] and Panchapakesan and Lumley [2]). (a) $u$-Component turbulence intensity. (b) $v$-Component turbulence intensity. (c) Turbulent kinetic energy $k$.

gases around $X/D_j = 40$. These values are in good agreement for the helium jet with the results obtained by Way and Libby [16] giving 28–30% in the $X/D_j$ range 15–20 and for air with those of Wygnanski and Fiedler [17] for $X/D_j > 30$ and also those of Chua [18] where $u'/(U_c-U_e) = 21\%$ at $X/D_j = 15$, but not so well with those of Champagne and Wygnanski [19]. If we extrapolate the present results to the far-field region, they are discordant with the measurements of Panchapakesan and Lumley [2] where $u'/U_c$ yields 40% at $X/D_j = 50$ for a free helium jet and 22% in air at $X/D_j = 30$. These differences in the turbulence level for the helium jet are explained by Panchapakesan

and Lumley who indicate that the flow configuration for Way and Libby's experiments is very close to the round plume region. This argument is not valid for the present investigation as the flow is studied far upstream ($X/D_j < 30$) of the plume region, which only begins at 73 $D_j$ for the helium jet. An effect of the thickness of the nozzle is also eliminated by the results of Matsumoto *et al.* [20] who show that such an influence may almost be ignored when the velocity of the primary jet is much larger than that of the external flow, as in the present experiments. The presence of a coflowing stream is supposed to be well taken into account through the non-dimensional presentation using $(U_c - U_e)$ and, indeed, using the work of Antonia and Bilger [21], one shows that when $U_j/U_c > 4.5$, as in the present case, almost no difference from a free jet is observed on the $u'/(U_c - U_e)$ axial evolution. Then, one of the last parameters to be considered to clear the asymptotic turbulence level is a possible confinement effect, in particular for the helium jet which expands rapidly. In order to qualify this influence, some measurements were made in free jets of air and helium with the Reynolds numbers defined in Table 1. These results show that the turbulence levels are very close to each other for the two free jets beyond $X/D_j = 30$, with an asymptotic value around 24% as found by So *et al.* [8] in premixed helium–air jet or Chua [18] in air jet beyond $X/D_j = 20$. The comparisons between the results obtained, with and without confinement, indicate that the presence of the confinement tends to increase the turbulence level on the jet axis. So, a confinement effect does not explain the discrepancy for the turbulence level with the helium free jet results of Panchapakesan an Lumley [2].

As the internal and external boundary layer characteristics, through their displacement thickness or their flow regime (laminar or turbulent), and the peak of turbulence intensity on the nozzle lip are the most important initial conditions driving the development of an axisymmetric shear layer [22], they are consequently the most likely parameters influencing the near-field of a jet and, as in the case of the shear layer, they may affect the far field turbulence level as well. Antonia and Bilger [21] have suggested this idea for jets. Most of the experiments are emulated with a laminar flow with a 'top-hat' velocity profile (Antonia and Bilger [21], Chua [18], Panchapakesan and Lumley [2]) with very different Reynolds numbers, but the influence of these parameters is not clearly established. Obviously, this problem deserves a systematic quantitative study as, for instance, the asymptotic value of $u'/(U_c - U_e)$ can be found in the literature, for instance in air free jets, in the range 22–29% without any clearly analysed reason.

The same remark is true for the radial velocity turbulent intensity, as $v'/(U_c - U_e)$ does not reach the plateau of 25% proposed by Wygnanski and Fielder [17], but is only around 22%, as Fig. 4b shows. The measurements of Chua [18] and Panchapakesan and Lumley [2] suggest that the value of the radial velocity turbulence intensity is not as large before $X/D_j = 30$. By another way, no comprehensive difference is observed between the evolutions of $v'/(U_c - U_e)$ in air or $CO_2$, so that the Reynolds number or the density variation seem to have a smaller influence on this quantity than on $u'/(U_c - U_e)$.

For symmetry reasons, statistics associated with $v'$ and $w'$ are equal on the jet axis. Then, the turbulent kinetic energy $k = 1/2\ (u'^2 + v'^2 + w'^2)$ is calculated by $k = 1/2\ u'^2 + v'^2$ and presented in Fig. 4c. The behaviour of $(2k/3)^{1/2}$ (chosen to be directly comparable with $u'$ as for isotropic conditions) is similar to the $u'$ evolution, reaching an asymptotic level more rapidly for the lighter gas. This rapid development is related to a more efficient entrainment by the helium jet. This result is not unexpected since it was shown [23] that the Strouhal number, which is used to characterise the size of the initial vortices, is also depending on the ratio $(\rho_j/\rho_e)^{1/2}$. These data showing that the helium jet tends to develop much more quickly than the others are also associated with the usual results for mixing layers, obtained from numerical simulations of the Brown and Roshko's experiments by Lummer (e.g. Fulachier *et al.* [24]) showing that, when the lighter fluid is on the side of the greater velocity, vortex pairing of the initial vortices is enhanced, thus increasing the mixing process.

2.1.3. *Skewness and flatness factor evolution.* Some effects also related to the considered gas are observed on the evolution of the skewness and flatness factors of the streamwise velocity fluctuations in this near-field region. The skewness factor evolution of the axial velocity $S_u$ is presented in Fig. 5 for the three gases on the jet axis. The measured value $S_u = -0.5$ at the nozzle exit is in good agreement with the skewness factor obtained from direct numerical simulations by Kim *et al.* [25] for a fully developed turbulent channel flow and for the three gases. A negative minimum of $S_u$ is found near the exit nozzle for $X/D_j < 10$. It appears at a shorter distance and with a smaller value for the lighter gas. This region corresponds properly to the potential core end where the axisymmetric mixing

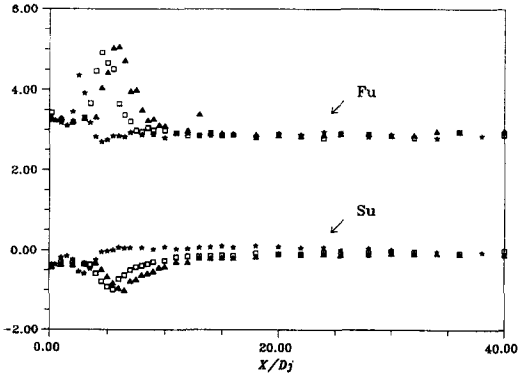


Fig. 5. Axial evolution of the $u$-component skewness $S_u$ and flatness $F_u$, symbols see Fig. 4c.

layer reaches the jet centreline. The negative sign of $S_u$ is linked to occasional incursions of external fluid, at low velocity, up to the axis. The flatness factor $F_u$ of the axial velocity component is given in Fig. 5 too. As for the skewness factor, the value of $F_u = 3.3$ at the nozzle exit agrees with Kim's results [25] for the three gases. These results tend to indicate that the initial conditions at the nozzle exit are the same for the three jets without any noticeable influence of the Reynolds number. Where a minimum of the skewness factor is observed, a maximum of the flatness factor occurs and the maximum of the axial turbulence intensity is reached (Fig. 4a). The influence of density on these quantities is obvious, showing, once more, that the initial axisymmetric mixing layer for helium develops and disappears very quickly. In the downstream field, the flatness factor reaches an asymptotic value $F_u = 2.8$ which indicates, complemented with a zero skewness factor, an almost-gaussian behaviour from $X/D_j = 15$, as it is found in the far-field of free jets where most of the experiments are usually performed.

2.1.4. *Velocity half-width distribution.* On the contrary, the velocity half-width $L_u$ is not very sensitive to the density variations. Figure 6 shows that the axial evolutions of $L_u$ for the three gases only slightly differ from each other. However, the behaviour of the helium jet is specific since an initial contraction ($2L_u/D_j = 0.81$ at $X/D_j = 3$) is observed for $X/D_j < 5$. For $X/D_j > 5$, the helium jet tends to spread more quickly than the heavier gases do. The latter result is the same as that obtained in the far-field region ($X/D_j > 50$) for a helium jet by Panchapakesan and Lumley [2], but this is not in agreement with the pseudo-similarity considerations which predict that $L_u$ would not depend on $\rho_j/\rho_e$. In addition to a slight density effect, this behaviour may be related to a Reynolds number effect, since it is known that the expansion of a jet with a lower Reynolds number jet is larger than that with a greater Reynolds number. However, the slopes of the linear dependence of $L_u/D_j$ on $X/D_j$ are lower in the present experiments than in the usual studies of free jets in the far-field. In the helium and air jets, the slope values obtained here are respectively

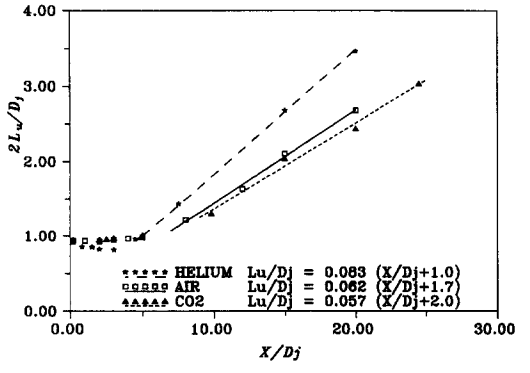


Fig. 6. Evolution of the mean longitudinal velocity half-width.

0.083 and 0.062, whereas Panchapakesan and Lumley [2] obtain 0.110 and 0.096. These discrepancies are probably related to the coflow presence and the relative wall proximity which both induce confinement effects which are not taken into account in this representation. Indeed, it was verified that the slopes for the helium and air free jets were, respectively, 0.109 and 0.092 in the present facility, in very good agreement with ref. [2]. Note that the discussed behaviour is opposite to that reported for a rectangular strongly heated (i.e. light) jet by Sahr and Gokälp [26]. Nevertheless, the main feature is that these length scales are only slightly affected, regardless of the different trends obtained by various authors (Fulachier *et al.* [4]), so that density does not influence these quantities as much as it influences the axial velocity decay rates: for instance, the ratio $(\rho_e/\rho_j)^{1/2}$ which is relevant for the velocity fall-off is as large as 2.7 for helium discharging into air, which is more than twice the observed difference on the jet spreading rates (1.3).

## 2.2. *Radial distributions*

2.2.1. *Mean longitudinal velocity.* The radial profiles of normalized mean longitudinal velocity $(U-U_e)/(U_j-U_e)$ are shown in Fig. 7a,b,c, respectively for the helium, air and $CO_2$ jets. Many different sections were investigated in the three gases in order to check the relevance of the effective diameter to describe and compare the radial evolutions of $U$ in gases with very different densities. These comparisons, not presented here, have shown that it is finally more interesting to compare the $U$-profiles at the same $X/D_j$ than at the same $X/D_{ef}$ in the studied near-field. This is directly linked to the fact that the radial expansion, which may be quantified through the half-width $L_u$, only weakly depends on the density variation, contrary to the axial velocity decay. At the jet exit, the velocity profile is far from the top-hat shape observed in many jet experiments, since it was chosen to work with fully turbulent developed characteristics to avoid any study of the transition in the near field. However the influence of the ejection conditions on the jet development would need some additional investigations with the hot wire technique for instance, since, owing to the slight inclination of the laser beam, no information about the $U$ velocity can be obtained by laser anemometry in sections closer than 0.2 $D_j$ from the nozzle exit. Some measurements made by static and head pressure tubes inside the nozzle at $X/D_j = -0.2$ in pure gas show that the $U/U_j$ profile is similar for the three gases and agrees with the fully turbulent developed Laufer's velocity profile [27] given in a tube following the standard 1/7 law. The representation in Fig. 7 gives a good overview of both the jet spread and the axial velocity decrease. One sees, for instance, that the radius where $U = U_e$ in the helium jet at $X/D_j = 20$ is $2R/D_j = 7$, which is not so far from the enclosure wall position ($2R/D_j = 11$) so that confinement effects are probably not negligible anymore at this station. Note that a linear extrapolation in the

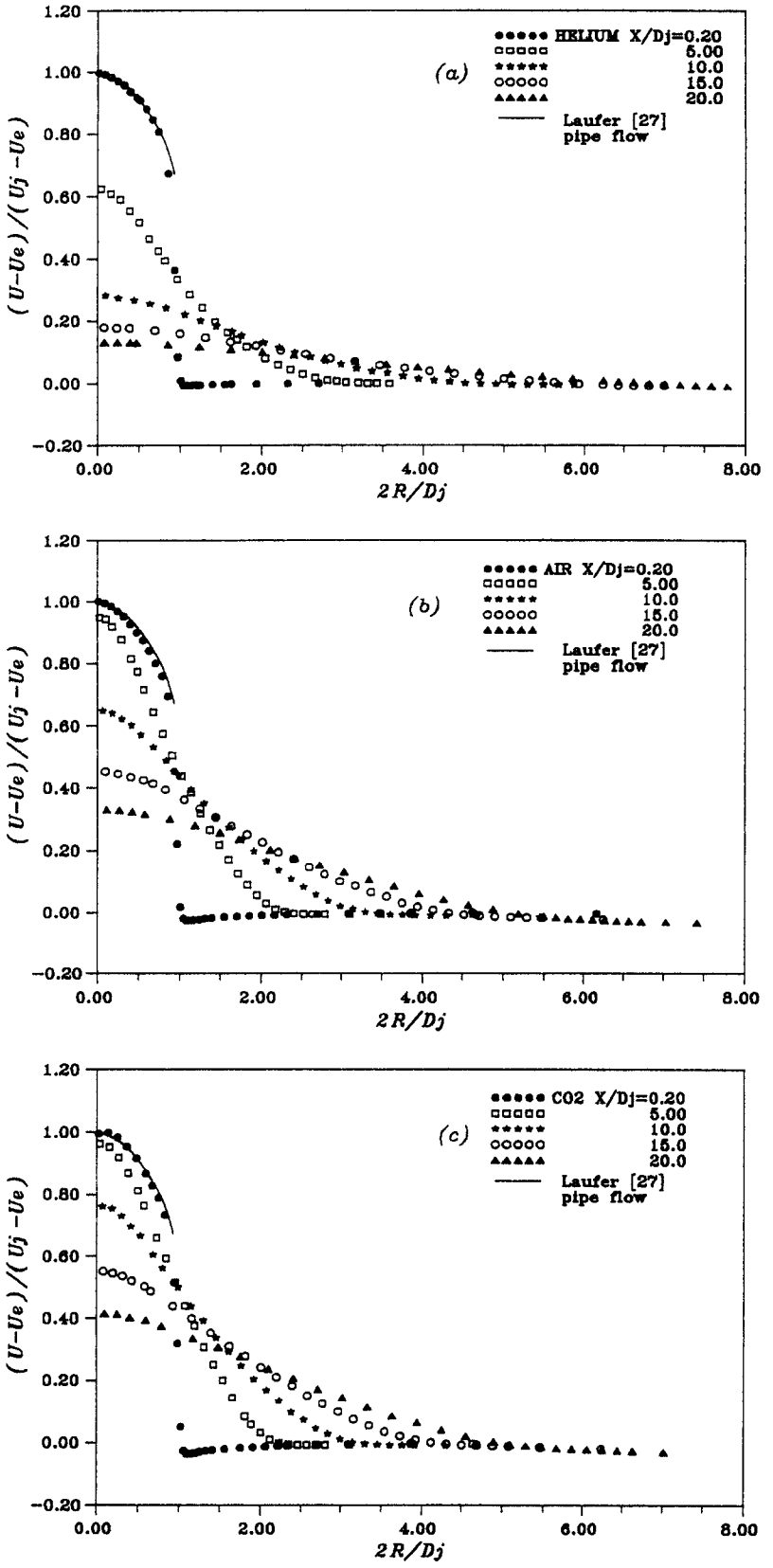


Fig. 7. Radial profiles of the mean longitudinal velocity: (a) in helium jet; (b) in air jet; (c) in $CO_2$ jet.

far-field of the jet boundary, where the velocity is equal to the local value of the external velocity, indicates that the helium would reach the wall at the station around $X/D_j = 28$. If the half-width $L_u$ is used for the non-dimensionalization, the usual relation $(U-U_e)/(U_c-U_e) = \exp(-(R/L_u)^2 \ln 2)$, used to described velocity profiles in similarity, fits well the radial profiles of $U$ for the three gases at $X/D_j = 15$ as presented in Fig. 8. Some slight discrepancies are observed for all three profiles. The external velocity $U_e$ used in the non-dimensional representation is here the local value in each section because, due to strong entrainment by the central helium jet, the external velocity $U_e$ begins to decrease at $X/D_j = 5$ from the initial conditions $U_e = 0.9$ m s$^{-1}$ and it reaches $U_e = 0.6$ m s$^{-1}$ at $X/D_j = 15$.

The mass flux $Q$ and, then, the entrainment $q = (Q-Q_j)/Q_j$, are deduced from the integration of the radial mean longitudinal velocity profiles in the various investigated sections. $Q$ is given by the expression

$$Q = \int_0^{R(U=U_e)} 2\pi r \rho (U-U_e)\, dr. \qquad (1)$$

Results presented in Fig. 9 for the air jet only indicate a parabolic dependence of $q$ on $X/D_j$ in the form $q = 5.0\ 10^{-3}\ (X/D_j)^2 + 0.13\ X/D_j$. This behaviour is quite different from the linear dependence of $q$ with the axial distance in the far-field ($q = 0.32\ X/D_j(\rho_j/\rho_e)^{-1/2}$ for $X/D_j$ in the range 50–400) given by Ricou and Spalding [28], but agrees rather well with the results presented by Hill [29] in the near-field for jets with high Reynolds numbers ($Re_j > 60\,000$) and also with the results of Boguslawski and Popiel [30] giving $q = 0.183\ X/D_j$ between 0 and $12D_j$. In fact, the evolution of $q$ seems to be almost linear in the very near and the far fields, but parabolic between them. The entrainment is lower in the present case than in free jets since, for instance, $q = 3$ is obtained at $X/D_j = 15$ instead of $q = 4$ at the same position in a free jet [29]. This shows that the coflowing stream and the enclosure affect the entrainment and obviously the jet development more than the Reynolds number does:

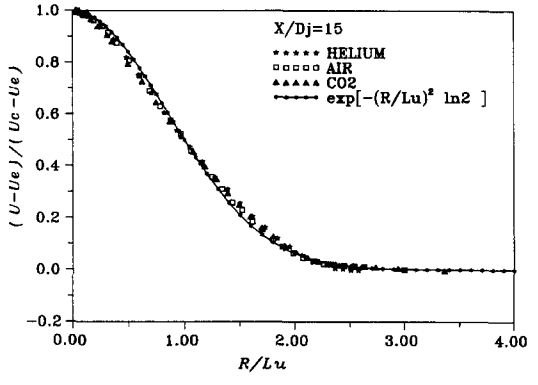


Fig. 8. Similarity of the mean longitudinal velocity in the section $X/D_j = 15$.

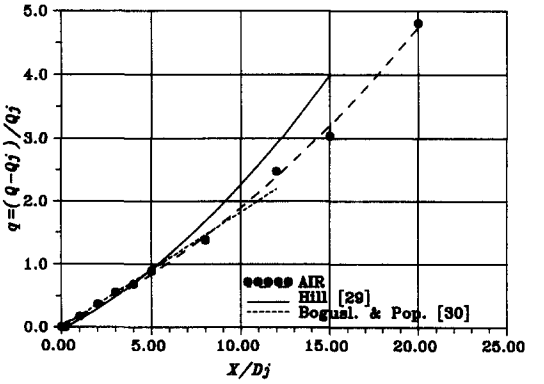


Fig. 9. Longitudinal evolution of the air jet entrainment.

a low Reynolds number, here $Re_j < 25\,000$, would induce stronger entrainment [28]. Note that entrainment is not presented here for the two other gases because its computation requires concentration measurements for the density calculation.

2.2.2. *Mean radial velocity.* Normalized mean radial velocity $V/(U_j-U_e)$ profiles are shown in Fig. 10 for the three gases at the section $X/D_j = 15$. Measurements of the radial mean velocity are rarely presented in experimental papers, because this component is a very difficult quantity to measure due to its low contribution to the velocity module. The radial distance where $V$ is positive is representative of the jet spread and it depends on the considered gas. Panchapakesan and Lumley [2] have calculated the self-similar $V$ profile in the far-field using the continuity equation. They have obtained a maximum of $V/U_c = 0.019$ at $R/X = 0.068$ (for $X/D_j > 60$), which is not so different from the present measurements at $X/D_j = 20$ giving a maximum $V/(U_c-U_e) = 0.023$ at $R/X = 0.073$. But the positive part of $V$ is reduced here when comparing our data with the previously cited experiments: this is in agreement with the fact that the entrainment and, consequently, the spreading are limited by the considered axial position $X/D_j$ and by an eventual confinement effect. As expected, the

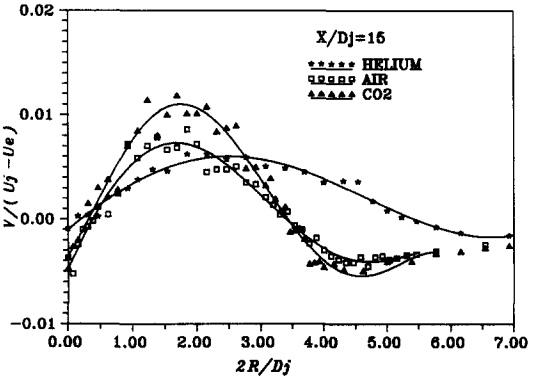


Fig. 10. Radial profiles of the mean radial velocity in the section $X/D_j = 15$.

mean radial velocity $V$ becomes negative in the outer region of the jet which means that some external fresh air is entrained by the central jet.

It is to be noted that the measurements of the radial velocity were particularly sensitive to the geometric adjustment of the laser beams with respect to the fictive axis of the jet. For instance, even though a good symmetry of the $U$ profile, a maximum of $U$ and a zero Reynolds stress $\langle uv \rangle$ were systematically checked on the axis, it was not possible in practice to simultaneously insure $V = 0$ everywhere on the axis from only one adjustment. Then, the determination of the radial mean velocity $V$ using the continuity equation is a good test of the measurement validity. The $V$ velocity is calculated in the experimental field of the air jet where the density is constant by

$$V(X, R) = -\frac{1}{R}\int_0^R r\frac{\partial U}{\partial x}\mathrm{d}r. \qquad (2)$$

The gradients $\partial U/\partial x$ are deduced from the cartography of $U(X, R)$ built by using the radial profiles of the mean axial velocity $U$ measured in 10 sections on the basis of information previously reported, ranging from the nozzle exit up to $X/D_j = 20$. A comparison of the measured and calculated values is given for various sections in Fig. 11. The best concordance is obtained beyond $2R/D_j = 1$ which shows that, on the jet side, where seeding may be a problem, the measurements of $V$ are quire reliable. The discrepancies observed near the axis are essentially due to the non-zero value of the measured $V$, whereas the calculated $V$ values are zero by symmetry considerations. Note that an arbitrary shift of the radial origin would give a better agreement of the measured $V$ values with the calculated ones.

2.2.3. *Velocity standard deviation.* The normalized axial and radial velocity standard deviations are plotted in Figs. 12a,b,c and 13a,b,c, respectively, for the three gases. The initial turbulent peak for $u'/(U_c - U_e)$ at $X/D_j = 0.2$ is larger for the lighter gas, because the mixing layer already begins to develop at this station

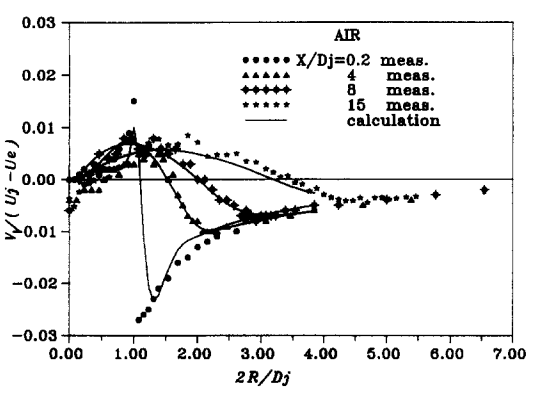


Fig. 11. Radial profiles of the mean radial velocity: comparison between measurements and calculation using the continuity equation in the air jet.

which corresponds to $X/D_{ef} = 0.54$ for the helium jet. The shape of the $u'$ profile begins to change at the end of the potential core, when the inner edge of the axisymmetric mixing layer reaches the axis. This is obtained at a shorter distance for the lighter gas (at $X/D_j \approx 3$ for the helium jet and 5 for the air and $CO_2$ jets). Then, the minimum of $u'/(U_c - U_e)$ on the axis quickly disappears for the helium jet and the profile tends to a self-similar shape from $X/D_j = 4.5$ with a nominal level around 27% on the axis. However, slightly greater values are obtained in the region $(R/L_u \approx 0.6)$ where turbulence production is maximum. This is in agreement with recent results for air jets [31]. As far as $v'/(U_c - U_e)$ is concerned, a minimum value is also obtained on the axis in the first investigated sections for the three gases as seen on Figs. 13a,b,c. However, it disappears earlier in terms of $X/D_j$ for $v'$ than for $u'$, namely, at $X/D_j = 12$ and 15 for the air and $CO_2$ jets, respectively. Note that this behaviour is not valid in the helium jet. At $X/D_j = 20$, which is in good agreement with Panchapakesan and Lumley's observations in the far-field, the $v'/(U_c - U_e)$ profiles for the three gases are not as different as the $u'/(U_c - U_e)$ are. For instance, at this station, they all present a similar shape up to around $2.7R/L_u$ with a maximum value on the axis of 16–18%. This confirms that, apart from the helium jet which has already reached a behaviour having similarity at $X/D_j = 20$, the $v'$ field is stabilised faster than the $u'$ one. The radial profiles of the azimuthal velocity component are not reported here as they are very close to those for the radial component.

The radial profiles of $(2k/3)^{1/2}$ given in Fig. 14, here using $k$ calculated by $k = 1/2(u'^2 + v'^2 + w'^2)$, tend to reach a shape in similarity from $X/D_j = 5$ in the helium jet with a value of $(2k/3)^{1/2}/(U_c - U_e) = 0.23$ on the axis. Figure 14a indicates that this behaviour is directly associated with the rapid obtainment of the asymptotic value of $(2k/3)^{1/2}/(U_c - U_e)$ in its axial evolution (see Fig. 4c). Moreover, the values of $(2k/3)^{1/2}/(U_c - U_e)$ are always greater in the helium jet by comparison with those in the air jet for the same sections, because of the differences previously observed on the $u'/(U_c - U_e)$ profiles.

The distributions of the Reynolds shear stress $\langle uv \rangle$ are given in Fig. 15a,b,c for the three gases. In the first sections, the maximum of $\langle uv \rangle/(U_c - U_e)^2$ is located at $R/L_u = 1$, and it is then slowly shifted towards $R/L_u = 0.8$ for downstream sections. The maximum level of $\langle uv \rangle/(U_c - U_e)^2$ only slightly depends on the considered gas and it is stronger for the lighter gas at any one section. An asymptotic maximum level $\langle uv \rangle/(U_c - U_e)^2 = 0.018$ is reached from $X/D_j = 15$ in the helium jet, which is in good agreement with the results of Panchapakesan and Lumley [2] obtained in a free jet at $X/D_j = 30$ (Fig. 15a). However, Fig. 16 shows that the correlation coefficient $\langle uv \rangle/u'v'$ is totally independent from the density variation at $X/D_j = 15$ since a very good collapse of the profiles is observed. It is to be noted, for instance, that a value

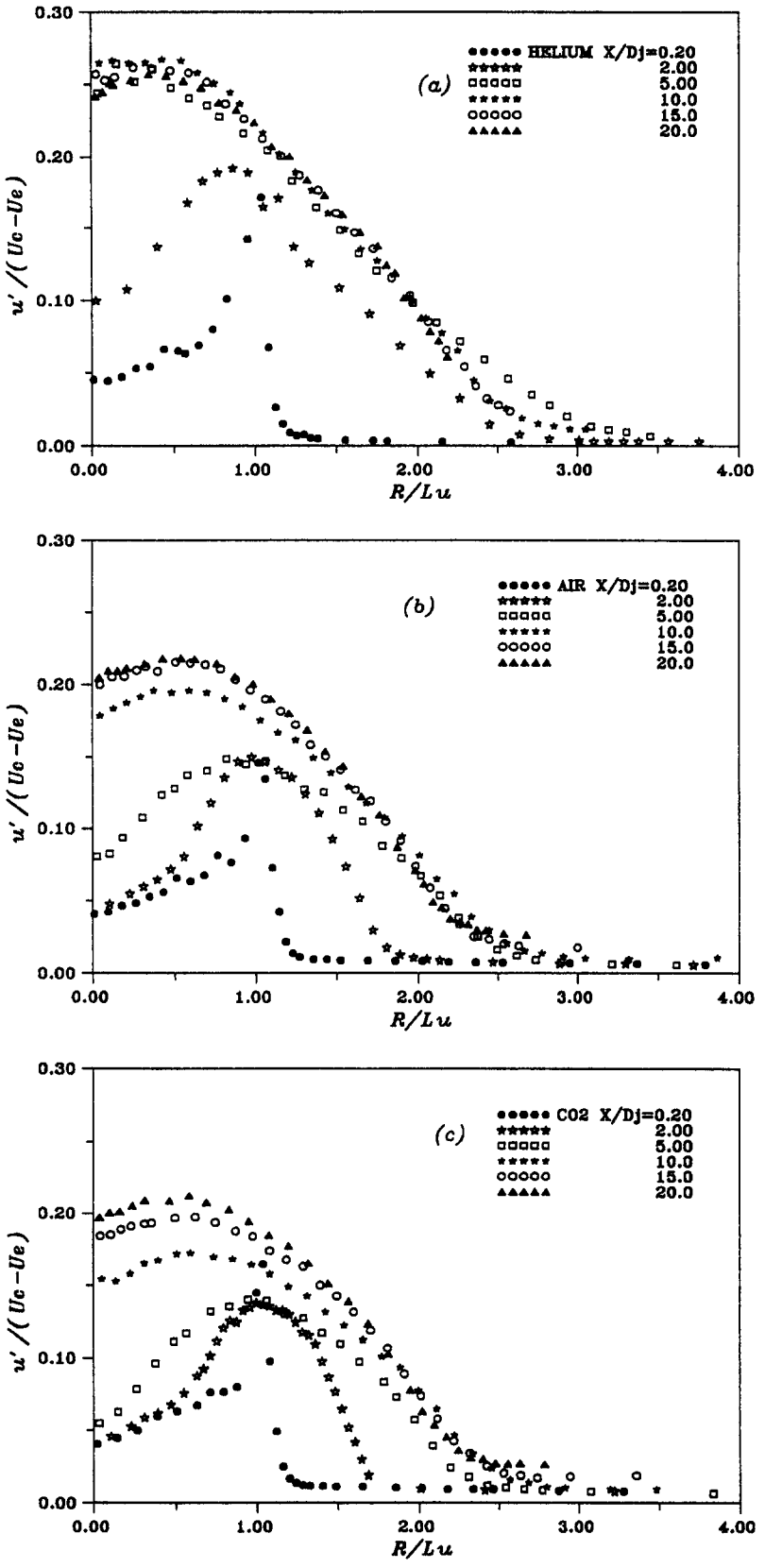


Fig. 12. Radial profiles of the $u$-root mean square: (a) in helium jet; (b) in air jet; (c) in $CO_2$ jet.

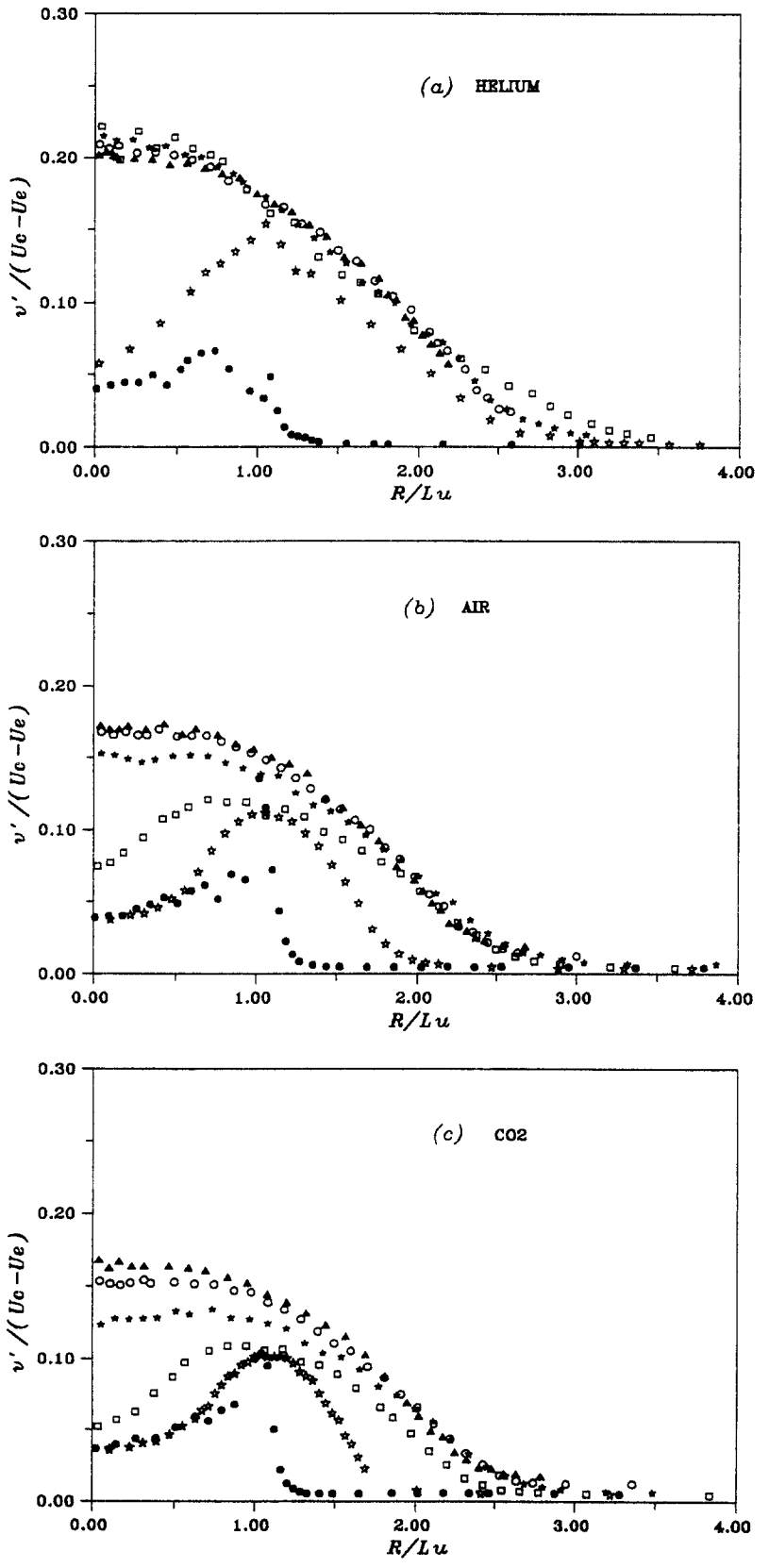


Fig. 13. Radial profiles of the $v$-root mean square, symbols see Fig. 12: (a) in helium jet; (b) in air jet (c) in $CO_2$ jet.

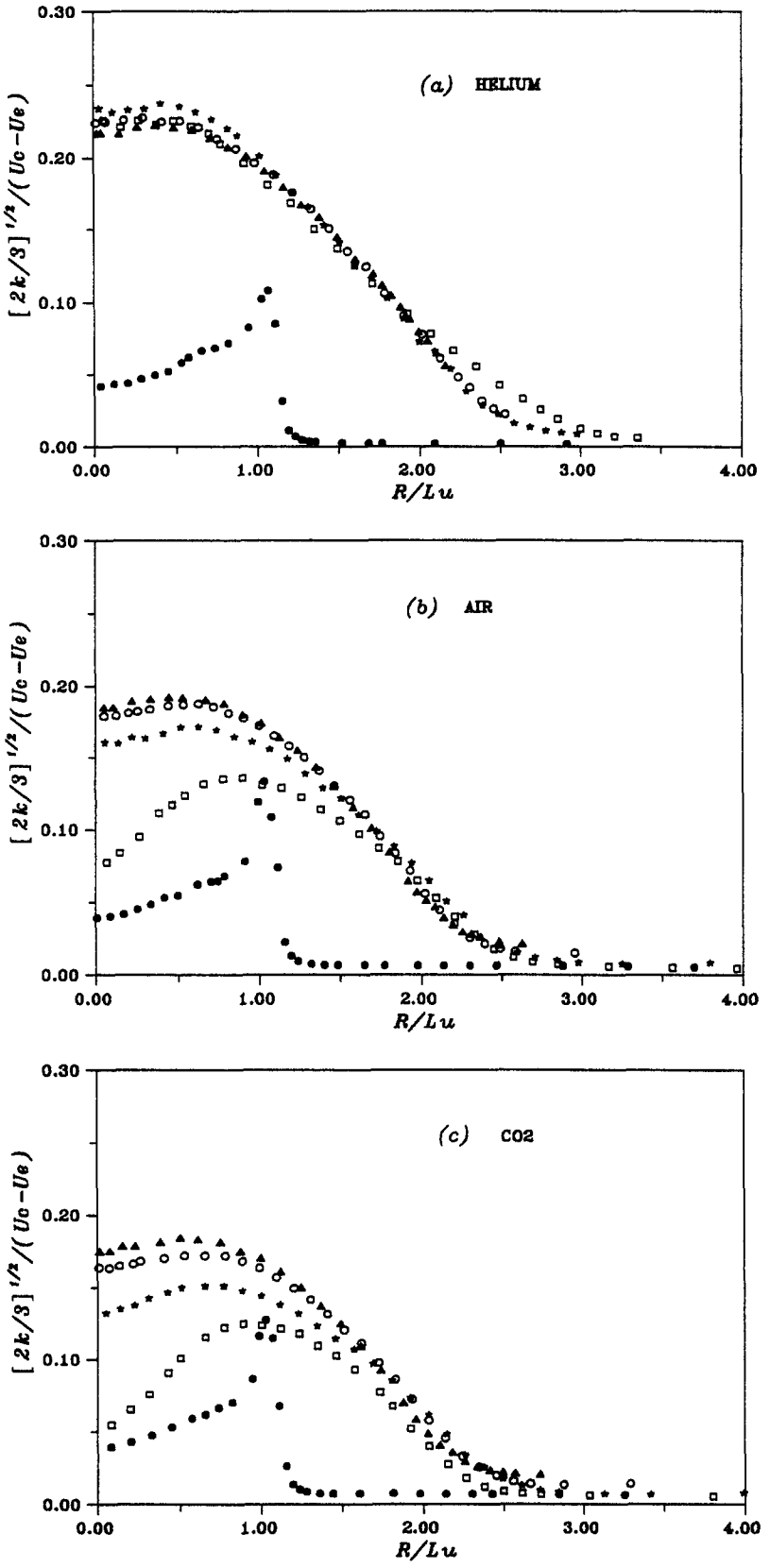


Fig. 14. Radial profiles of the turbulent kinetic energy, symbols see Fig. 12: (a) in helium jet; (b) in air jet; (c) in $CO_2$ jet.

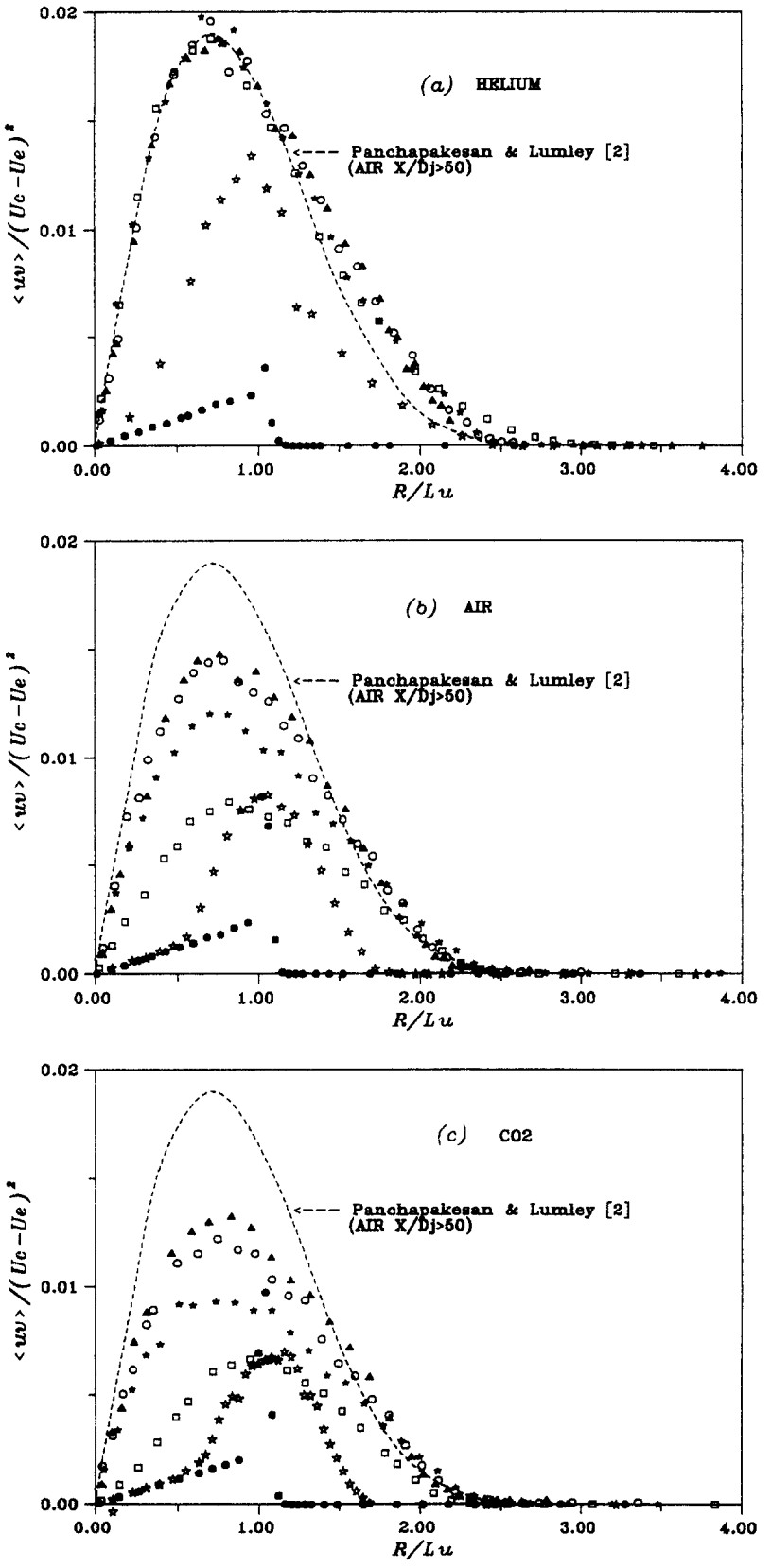


Fig. 15. Radial profiles of Reynolds shear-stress, symbols see Fig. 12: (a) in helium jet; (b) in air jet (c) in $CO_2$ jet.

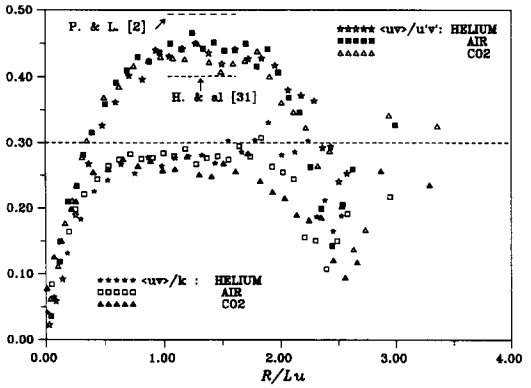


Fig. 16. Radial profiles of the $\langle uv \rangle$ correlation coefficient and of the ratio $\langle uv \rangle / k$ in section $X/D_j = 15$.

of about 0.45 is maintained over a large $R/L_u$ range, namely, between 0.8 and 1.8. Such a plateau is obtained in most of the turbulent shear flows. In particular, this result is in agreement with the values of the correlation coefficients deduced from the measurements of Panchapakesan and Lumley [2] as well as from those of Hussein *et al.* [31]. The evolution of the ratio $\langle uv \rangle / k$, called structure parameter, is also presented in Fig. 16 for $X/D_j = 15$. The shape of the profile remains the same for the three gases with a plateau over the region around $R/L_u = 1$ at the level of $\langle uv \rangle / k \approx 0.28$ when the Reynolds stress $\langle uv \rangle$ and the turbulent kinetic energy production are maximum. A value around 0.3 of this parameter is usually obtained in fully turbulent flows. For $R/L_u > 1$, $\langle uv \rangle / k$ increases up to 0.32 at $R/L_u = 2$ and then decreases in the outer part of the jet, due to the intermittence.

## 3. CONCLUSION

This paper has reported detailed measurements of the turbulent velocity field in the near-field region of variable density jets. It was shown that the initial density ratio strongly affects the development of these jets. In the asymptotic state, the centreline mean velocity is also strongly influenced by this parameter, whereas the turbulent field is almost independent from it. Other characteristics of the flow like the Reynolds number, the confinement or the coflow also influence the jet development, but to a much smaller extent. A lighter gas tends to mix more quickly with the ambient one than a heavier gas does, and this trend is confirmed for jets either with the same momentum flux or the same Reynolds number. More specifically, the large scales of the flows like the velocity half-width are rather weakly influenced by the density variation, and the turbulence levels are almost the same for the three studied gases in stations located beyond $X/D_j = 20$. This behaviour may be related to the choice of the same momentum flux as the control parameter since the far-field values of all the centreline characteristic length scales are then equal in the three gas flows with very different densities [1].

As the instantaneous velocity data were systematically stored, the budget for the turbulent kinetic energy equation can now be established by calculating the triple moments. Determining this budget in several sections of the near-field region will give some insight into the way the different components of the balance are gradually evolving towards those displayed by Panchapakesan and Lumley [2] in the far-field region. The mean concentration fields in helium and $CO_2$ jets, which have already been measured, will then be used for this calculation and for the determination of other global quantities such as the entrainment. These perspectives will be the objective of a next paper.

*Acknowledgements*—This work was supported by Electricité de France, Gaz de France, Société Nationale de Construction de Moteurs d'Avions, Institut National de l'Environnement Industriel et des Risques and Conseil Régional Provence-Alpes-Côte d'Azur. The authors also wish to acknowledge M. M. M. Astier and P. Bonnelye for their help in the design and the construction of the test facility.

## REFERENCES

1. E. Ruffin, R. Schiestel, F. Anselmet, M. Amielh and L. Fulachier, Investigation of characteristic scales in variable density turbulent jets using a second-order model, *Phys. Fluids* **6**, 2785–2799 (1994).
2. N. R. Panchapakesan and J. L. Lumley, Turbulence measurements in axisymmetric jets of air and helium—Part 1, air jet; Part 2, helium jet, *J. Fluid Mech.* **246**, 197–223, 225–247 (1993).
3. P. Huerre and P. A. Monkewitz, Local and global instabilities in spatially developing flows, *A. Rev. Fluid Mech.* **22**, 473–537 (1990).
4. L. Fulachier, F. Anselmet and M. Amielh, Quelques résultats sur les écoulements subsoniques à masse volumique variable, *27ème Coll. Aérodyn. Appl.* (1990).
5. F. C. Gouldin, R. W. Scheffer, S. C. Johnson and W. Kollman, Nonreacting turbulent mixing flows, *Prog. Energy Combust. Sci.* **12**, 257–303 (1986).
6. W. M. Pitts, Effects of global density and Reynolds number variations on mixing in turbulent axisymmetric jets, NBSIR 86-3340, National Bureau of Standards, US Department of Commerce (1986).
7. C. D. Richards and W. M. Pitts, Global density effects on the self-preservation behaviour of turbulent free jets, *J. Fluid Mech.* **254**, 417–435 (1993).
8. R. M. C. So, J. Y. Zhu, M. V. Ötügen and B. C. Hwang, Some measurements in the binary gas jet, *Exp. Fluids* **9**, 273–284 (1990).
9. R. K. Chen and W. Rodi, *Vertical Turbulent Jets*. Pergamon Press, Oxford (1980).
10. P. Bonnelye, Conception et réalisation d'une soufflerie subsonique pour l'étude des écoulements à masse volumique variable, Thèse CNAM, Univ. Aix-Marseille II, IMST (1991).
11. M. Coantic, Contribution à l'étude de la structure de la turbulence dans une conduite de section circulaire, Thèse de Doctorat ès-Sciences Physiques, Univ. Aix-Marseille (1966).
12. F. R. Steward and A. G. Guruz, Aerodynamics of a confined jet with variable density, *Combust. Sci. Technol.* **16**, 29–45 (1977).
13. P. G. Gladnick, A. C. Enotiadis, J. C. LaRue and G. S. Samuelsen, Near-field characteristics of a turbulent coflowing jet, *AIAA J.* **28**, 1405–1414 (1990).

14. J. C. Sautet, Effects des différences de densité sur le développement scalaire et dynamique des jets turbulents, Thèse de Doctorat, Université Rouen (1992).
15. M. W. Thring and M. P. Newby, Combustion length in enclosed turbulent jet flames, *4th International Symposium Comb.* (1952).
16. J. Way and P. A. Libby, Application of hot-wire anemometry and digital techniques to measurements in turbulent helium jet, *AIAA J.* **9,** 1567–1573 (1971).
17. I. J. Wygnanski and H. E. Fiedler, Some measurements in the self-preserving jet, *J. Fluid Mech.* **38,** 577–612 (1969).
18. L. P. Chua, Measurements in a turbulent circular jet, Ph.D. Thesis, University Newcastle (Australia) (1989).
19. F. H. Champagne and I. J. Wygnanski, An experimental investigation of coaxial turbulent jets, *Int. J. Heat Transfer* **14,** 1445–1464 (1971).
20. R. Matsumoto and K. Kimoto, A study on double concentric jets, *Bull. JSME* **16,** 93 (1973).
21. R. A. Antonia and R. W. Bilger, An experimental investigation of an axisymmetric jet in a co-flowing air stream, *J. Fluid Mech.* **6,** 805–822 (1973).
22. A. K. M. F. Hussain and M. F. Zedan, Effects of the initial condition of the axisymmetric free shear layer: effect of the initial fluctuation level, *Phys. Fluids* **21,** 1475–1481 (1978).
23. H. G. Green and J. H. Whitelaw, Velocity and concentration characteristics of the near-field of round jets, *Coll. EUROMECH* 237, Marseille (1988).
24. L. Fulachier, R. Borghi, F. Anselmet and P. Paranthoen, Influence of density variations on the structure of low-speed turbulent flows, *J. Fluid Mech.* **203,** 577–593 (1989).
25. J. Kim, P. Moin and R. Moser, Turbulence statistics in fully developed channel flow at low Reynolds number, *J. Fluid Mech.* **177,** 133–166 (1987).
26. B. Sahr and I. Gökalp, Variable density effects on the mixing of turbulent rectangular jets, *Eighth Symposium on Turbulent Shear Flow*, Vol. 1, pp. 641–646 (1991).
27. J. Laufer, The structure of turbulence in fully developed pipe flow, NACA REPORT/1174 (1953).
28. F. P. Ricou and D. B. Spalding, Measurement of entrainment by axisymmetrical turbulent jets, *J. Fluid Mech.* **11,** 21–32 (1961).
29. B. J. Hill, Measurement of local entrainment rate in the initial region of axisymmetric turbulent air jet, *J. Fluid Mech.* **51,** 773–779 (1972).
30. L. Boguslawski and Cz. O. Popiel, Flow structure of the free round turbulent jet in the initial region, *J. Fluid Mech.* **90,** 531–539 (1979).
31. J. H. Hussein, S. P. Capp and W. K. George, Velocity measurements in a high-Reynolds number, momentum-conserving, axisymmetric, turbulent jet, *J. Fluid Mech.* **258,** 31–75 (1994).